Geological and mineralogical controls on landslide formation: A case study from the Birgha Bhanjyang Landslide, Syangja District, Gandaki Province, Nepal

Ashok Sigdel*, Sushan Upadhyay, Subash Acharya & Champak Babu Silwal

Department of Geology, Tri-Chandra Multiple Campus, Tribhuvan University, Kathmandu 44605, Nepal; ashok.sigdel@trc.tu.edu.np
*Corresponding Author: Ashok Sigdel

AGEOS

Abstract: Birgha Bhanjyang landslide, located in the Syangja district of central-west Nepal, is among the most active slope failures in the region. While it is primarily triggered by intense monsoonal rainfall, its evolution is strongly influenced by weak lithology, structural discontinuities, and prolonged rock weathering. Geological investigations reveal that the landslide zone consists mainly of highly weathered shale and phyllite, interbedded with quartzite and minor quartz veins. Geophysical surveys using Electrical Resistivity Tomography (ERT) indicate a thick residual and colluvial cover resting above fractured and weathered bedrock, with distinct shear zones at several depths. These shear zones reflect the presence of the Badi Gad fault, which cuts across the area, contributing to mechanical fracturing and accelerating weathering processes in the rock mass. Mineralogical analysis through X-ray Diffraction (XRD) confirms the presence of clay minerals such as quartz, illite, chlorite, and kaolinite, all products of prolonged chemical and mechanical weathering. Petrographic studies further support these findings, showing feldspar alteration and the branching pattern of biotite decomposition caused by chemical mineral alteration. The geotechnical properties of the soil also show the evidence of ongoing rock disintegration. Altogether, these results highlight that the Badi Gad fault plays a dominant role in driving both mechanical and chemical weathering of the rocks, making it the principal factor behind the instability of the Birgha Bhanjyang slope.

Key words: Birgha Bhanjyang landslide, clay mineralogy, weathering, electrical resistivity tomography, Badi Gad Fault

1. INTRODUCTION

In situ weathering of bedrock generates residual soils whose engineering properties are controlled by a complex interplay of lithology, climate, hydrology, geomorphology, and vegetation (Wesley, 2010; Inrdawan et al., 2024; Hossain et al., 2025). Unlike transported soils, residual soil retains the mineralogical and structural signatures of their parent rocks, where alteration of feldspars, micas, and other silicates commonly yields secondary clays such as kaolinite, smectite, illite, chlorite, and mixed-layer assemblages (Wang et al., 2024). This mineralogical evolution is strongly associated with decreases in density, shear strength, and overall stability of the slope (Brenner et al., 1985; Calcaterra and Parise, 2005; Sajinkumar et al., 2011; Regmi et al., 2012). Other studies further show that cracks (both macro and micro) developed due to chemical alteration processes together with fractures and discontinuities generated by fault mechanism enhance porosity and permeability in bedrock resulting in preferential weathering of steep slopes (Gerber & Scheidegger, 1969, Park et al., 2024). Numerical models also confirm that interactions between water bodies and rock, along fractures, dissolve minerals, enlarge flow pathways play a vital on fault and fracture geometry and their pace and extent of chemical alteration (Yu, 2019).

In the Nepal Himalaya, a natural laboratory of intensely weathered metamorphic sequences, field, petrographic, clay minerals, and geotechnical studies show how these micro- to meso-scale processes control the slope behavior linked with fault movement (Neupane and Adhikari, 2011; Regmi et al., 2012). Mineralogical and geochemical investigations have identified assemblages of illite, chlorite, kaolinite, and mixed-layer clays within weathered zones that correlate with slope failures (Silwal et al., 2024). During weathering, biotite and feldspars are altered into clay minerals such as illite, chlorite, kaolinite and other mixed layers clay, forming the most significant mineralogical change in the rocks. This alteration facilitates rock breakdown along joints and fractures, and when combined with physical erosion and tectonic activity, can lead to slope failure. The presence of smectite or mixed-layer illite–smectite in phyllite- and shale-derived soils under saturated conditions is particularly detrimental, as it reduces shear strength and enhances susceptibility to reactivation of landslides during monsoon (Panthee et al., 2023).

This study examines the relationship between the physical and chemical weathering of rocks and minerals and their direct influence on landslide in the Lesser Himalaya of Nepal. For this purpose, we focus on the Birgha Bhanjhyang landslide—locally known as *Biramdi Pahiro*—situated in Kaligandaki Rural Municipality of Syangja District, western Nepal. This landslide is recognized as a long-standing, recurrent slope failure with a history of more than three decades, posing ongoing risks to the community of Birgha Archale village. The lithology of the area is predominantly composed of metamorphic rocks, which display considerable variability due to their heterogeneous composition and differing degrees of weathering (Dhital et al., 2002). Previous studies have largely emphasized the geology and structural

Manuscript received 2025-10-19
Revised version accepted 2025-12-22

patterns of the area (DMG, 1983; Sakai, 1985; Timalsina and Poudyal, 2018), but no comprehensive research has yet integrated geological, mineralogical, and geotechnical perspectives to understand the weathering processes and their role in the formation of the Birgha Bhanjhyang landslide. Therefore, this study aims to investigate both physical and chemical weathering of rocks and soils by employing geological and mineralogical proxies alongside geotechnical characterization, in order to elucidate the development of this landslide.

2. STUDY AREA

The Birgha Bhanjhyang landslide is situated in Ward No. 4 of Kaligandaki Rural Municipality, Syangja District, within Gandaki Province of western Nepal. Geographically, the site is located at 27°57'02.33"N latitude and 83°33'15.26"E longitude (Fig.1). The elevation in the study area ranges from approximately 300 meters near the banks of the Kaligandaki River to about 950 meters. The topography varies significantly from steep hillslopes to relatively flat river terraces along the Kaligandaki River valley. The landscape is characterized by distinct geomorphic features including ridges, spurs, gullies, and saddles. The drainage system is dominated by the Kaligandaki River, the principal river in the area, and is supplemented by other minor tributaries in the vicinity of the study area. Notably, the Birgha Bhanjyang landslide body itself contributes to the local drainage system, acting as a channel for surface runoff during monsoon periods.

3. REGIONAL GEOLOGY

Geologically, the study area mainly consists of Galyang, Sangram, Syangja, Lakharpata, Swat, and Suntar Formations (DMG, 1983). The Galyang Formation predominantly comprises dark grey shale associated with black limestone, calcareous slate, and subordinate dolomitic limestone. The Sangram Formation is characterized by grey to greenish calcareous shale with intercalations of limestone. Similarly, the Syangja Formation consists of quartzite of varying colors accompanied by variegated shale. The Lakharpata Formation is composed of fine-grained grey to pink limestone and dolomitic limestone interbedded with purple and greenish shale. The Swat Formation mainly includes grey to dark grey shale with fossiliferous limestone, while the Suntar Formation comprises fine- to medium-grained greenish sandstone intercalated with greenish shale.

Among these formations, the Birgha Bhanjyang Landslide lies within the Galyang and Syangja Formations of the Lesser Himalayas in west-central Nepal (Fig. 2). This formation is correlated to the Sorek Formation of the Sirkot Group, which includes red-purple to grey-green shale or slate and pale yellow, pink, or grey quartzite (Dhital, 2015). A major east-west trending strike-slip fault, called the Badi Gad Fault, runs through the landslide area (Sakai, 1985). The Badi Gad-Kali Gandaki Fault follows the Badi Gad Khola in the west and continues along the Kali Gandaki valley in the central and eastern parts of the study area (Sakai, 1985; Dhital et al., 2002; Timalsina and Paudyal, 2018). According to Paudel (2012), the Badi Gad-Kali Gandaki

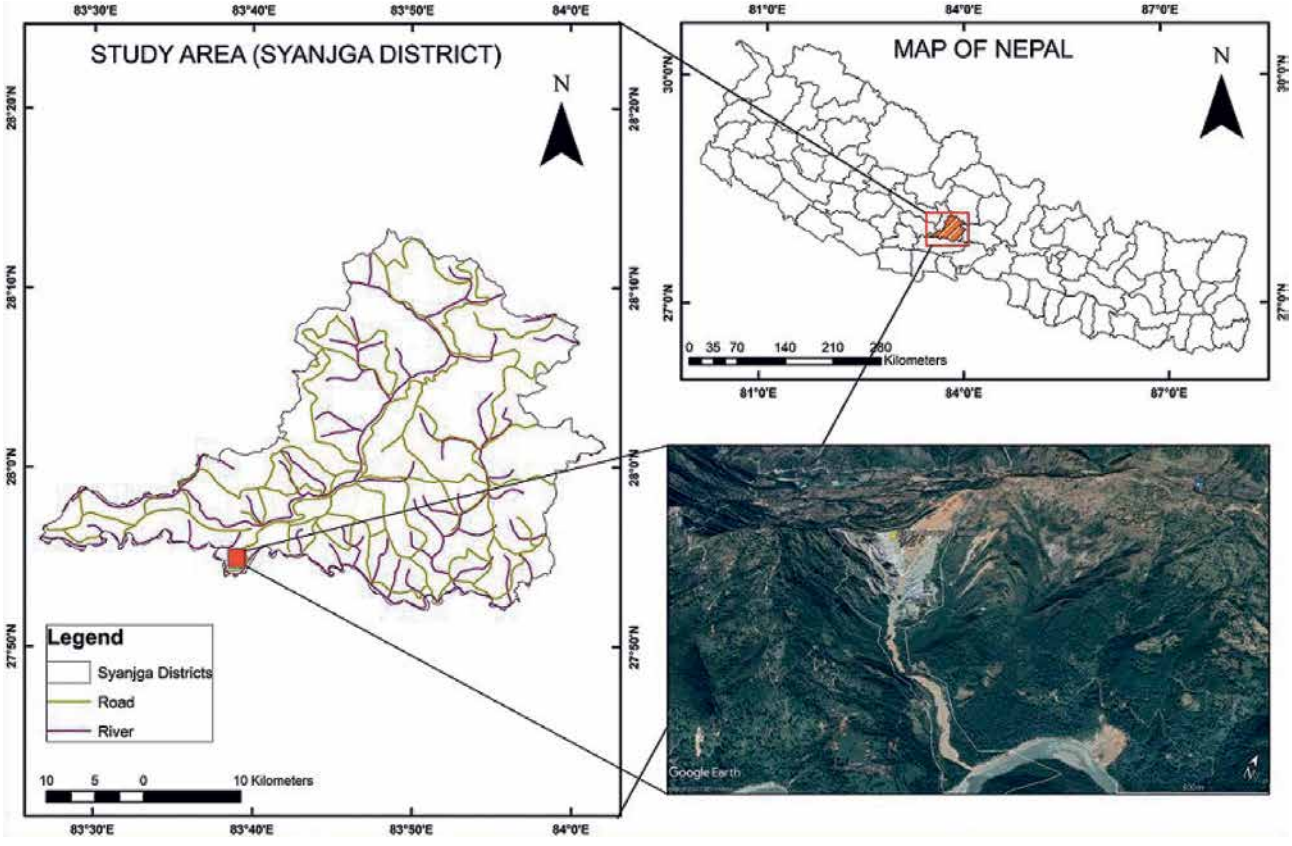

Fig.1: Location Map of the Study area. The red square indicates the location of the Birgha Bhanjyan landslide which is shown in Google Earth image.

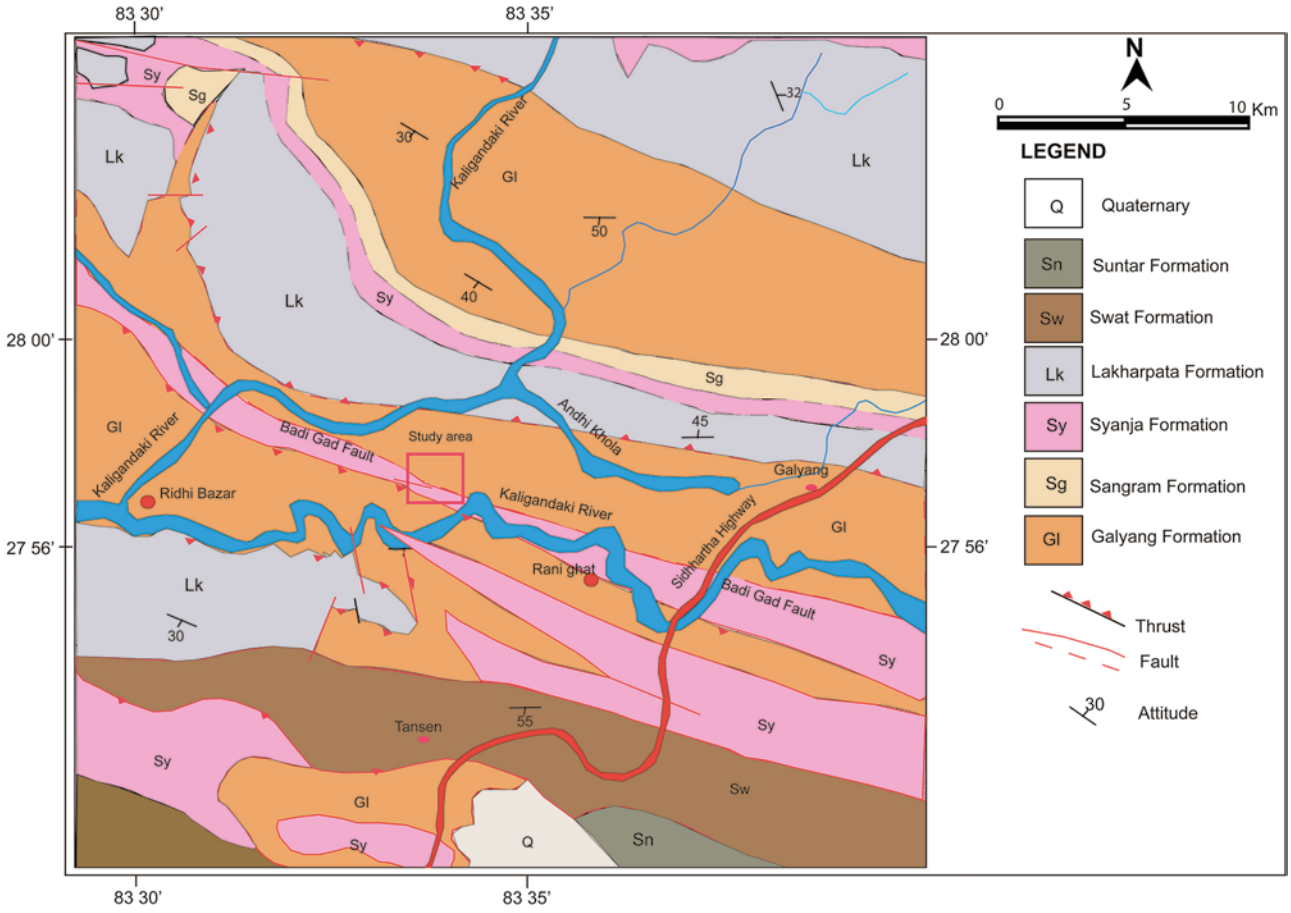

Fig. 2: Generalized Geological Map of the study area. (Modified from DMG, 1983, the name Badi Gad Fault is taken from Sakai, 1985 and Timalsina and Paudyal, 2018)

Fault (BKF) is one of the most noticeable and clearly visible structural features in the western Nepal. When this fault cuts across mountain ridges, it frequently creates broad depressions and contributes to the development of active landslides.

4. METHODS

Geological investigation of the Birgha Bhanjyang landslide involved detailed field observations of exposed outcrops to document lithology, discontinuity patterns, weathering condition, rock mass strength, and seepage conditions.

Electrical Resistivity Tomography (ERT) was performed to identify the subsurface information and shear zone caused by the active Badi Gad fault. The survey alignment was designed to make it cross over as a perpendicular to the fault line. A profile length of 300 m with electrode spacing 5 m by Wenner array is used during the field survey to collect subsurface information of at least 30 m depth. Two ERT lines (ERT 1 and ERT 2) were set across the fault line near the crown and toe of the landslide to cover the maximum landslide area (Fig.3).

A total of six soil samples labelled as S1, S2, S3, S4, S5, S6 were collected from the landslide area (two from the crown, three from the main body and one from the toe part). These soil samples were further analyzed to investigate the geotechnical parameters of the soil and also for X-ray diffraction (XRD). Four rock samples from the body part of the landslide were collected for petrographical analysis (Fig. 4)

Clay Mineralogical analysis was carried out by X-ray diffraction (XRD) with a Bruker D8 Phaser (Cu-Kα, λ = 1.5406 Å) at Nepal Academy of Science and Technology (NAST), Kathmandu, Nepal. Similarly, petrographical analyses were carried out using thin-section petrography under a polarizing microscope at the Department of Mines and Geology (DMG), Kathmandu, Nepal.

The geotechnical characterization included grain size analysis (sieve method, USCS classification), Atterberg limits (ASTM D4318-84), specific gravity (ASTM D854-93), and moisture content (ASTM D2216-92). Soil shear strength parameters—cohesion (c) and internal friction angle (φ)—were determined by direct shear tests conducted under varying normal stress. Besides these, void ratio, porosity, and density tests were calculated to describe the soil's compactness and permeability characteristics. Lastly, unit weight is vital for understanding overburden stress and pressure distribution within soil layers.

5. RESULTS

5.1 Characterization of the Landslide

The Birgha Bhanjyang landslide is facing southeast and is characterized by the presence of residual and colluvial soils

Fig. 3: Location of the ERT lines in Google Earth where red das line indicates the Badi Gad Fault and orange das line boundary indicates active landslide area. Upper photograph shows the close view of landslide area.

overlaying the bedrock. The slope gradient varies between 50° and 80°. Geologically, the area lies within the Precambrian rocks of the Lesser Himalaya, specifically the Galyang and Syangja Formations of the Midland Group (DMG, 1983). The lithology comprises weathered, sheared, and fractured shale and phyllite with interbedded slate and quartzite, often showing boudinage type and folded structures. These rocks are oriented towards NW to SW and dipping toward NE. Badigad Fault evidence by sheared materials and regional geological mapping (DMG, 1983; Sakai, 1985), passes through the area. The engineering geological map of the landslide and its surrounding area is shown in Fig. 4. The Birgha Bhanjyang landslide has two large scarps developed in each of the tributaries of the Phairo Khola and they coalesce downstream (Fig. 5A). The top of the slide reaches the Birga Archale, while its toe lies at the cut bank of the Kaligandaki River (Fig. 4).

The crown extends towards the right flank and mainly consists of residual soil. The residual soil at the crown exhibits high porosity, which facilitates moisture retention, while the colluvium, composed of materials ranging from small pebbles to cobbles and boulders, exhibit high permeability (Fig.5B). The thickness of the residual soil and colluvium is about 20-25 m. A large scrap is present along the crown. The slope angle of the crown to middle part is 50-80°. Several cracks are also present around the crown. The morphology of the crack is about 5-10 m in length, width 2-5 cm and depth 1- 1.5 m (Fig. 4).

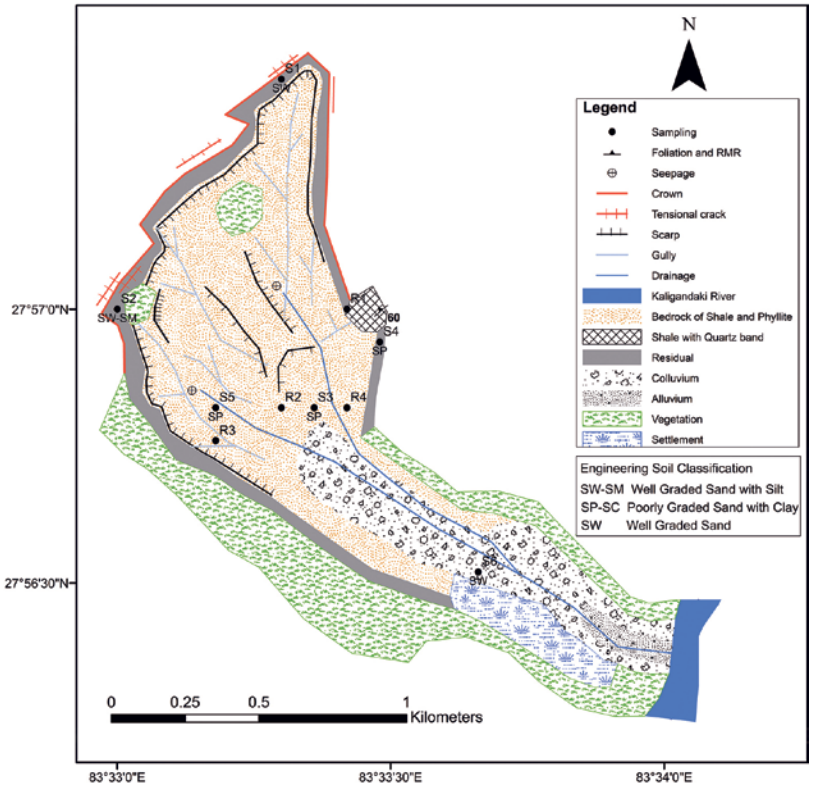

Fig.4: Engineering Geological Map of the Birgha Bhanjyang landslide

The central part of the landslide is covered by a very thin layer of colluvial deposits comprising pebbles, cobbles, and boulders, which were primarily derived from shale and quartzite beds. In addition, the landslide body exhibits extensive coverage of very loose, intensely weathered, and highly sheared rock, including jointed grey to greenish-grey and reddish-brown phyllites and shales (Fig.5 C-E). The extensive weathering of these rocks has nearly transformed into soil (Fig.5D). Quartzite and associated quartz veins are highly fractured and folded (Fig.5C). This fractured pattern is associated with a fault passing through the landslide. The slope gradient in the middle section of the landslide is 40°-50°. Rill and gully erosion are evidence of active surface processes. Several scars are developed around the body part of the landslide.

The toe section of the landslide is predominantly composed of colluvial and debris flow deposits, which have been transported by the Pahiro Khola, a local stream that eventually converges with the Kaligandaki River (Fig.5F). The materials at the toe

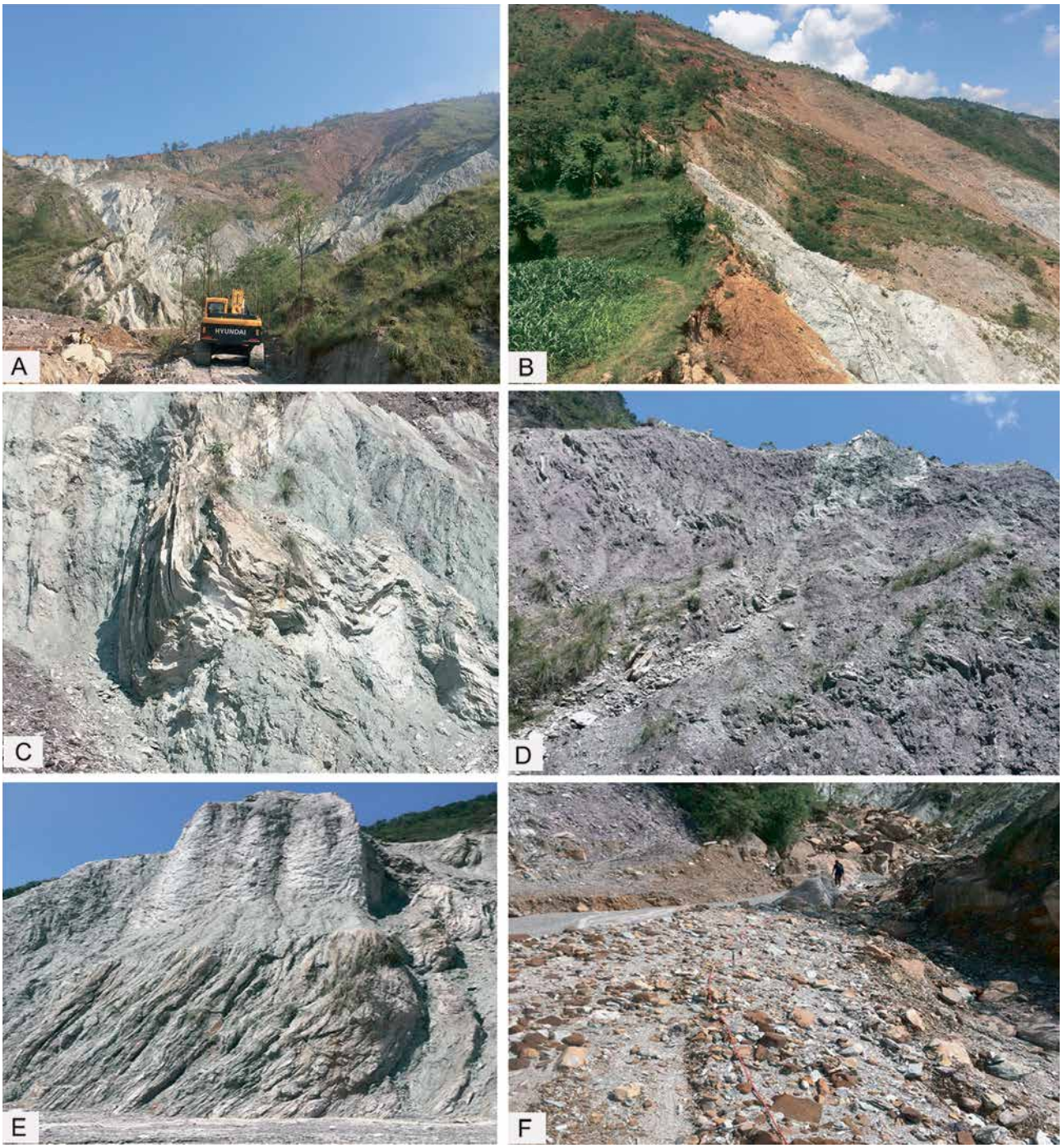

Fig.5 Field Photograph of the different parts of the landslide A) Overall view of the landslide B) Residual soil and colluvium with scarp in the Crown part. C) Highly deformed and folded quartzite beds in the central part of the landslide D) Highly weathered Red purple shale at central part E) Highly weathered and sheared Phyllite F) Colluvial deposits at the toe part of the landslide

include a heterogeneous mixture of pebbles, cobbles, and large boulders about 10 m thick.

5.2 Electrical Resistivity Tomography (ERT) of the Landslide area

The Electrical Resistivity Tomography (ERT) survey was carried out using a Wenner array configuration with an electrode spacing of 5 m. Data acquisition was performed with a GD-10 resistivity meter, and the dataset was processed using 2D tomographic inversion techniques in the Res2DInv software. The ERT profiles were positioned across the fault traces, as illustrated in Fig. 3.

In ERT-1, the tomogram clearly displays a sharp vertical resistivity contrast at approximately 110 m and 190 m, interpreted as a fault zone. The shear zone is distinctly visible, characterized by very low resistivity values. Resistivity values ranging from 30–100 Ωm correspond to highly weathered and fractured shale and phyllite, whereas high resistivity values (>1000 Ωm) are associated with quartzite and intact phyllite bedrock (Fig.6A). Similarly, ERT-2 also reveals a pronounced resistivity contrast. On the NE side, relatively low resistivity values (>25 Ωm) represent intensely weathered and fractured bedrock (Fig. 6B), while the SW side shows quartzite and phyllite bedrock with higher resistivity (around 220 Ωm). In both tomograms, the transition between weathered, fractured bedrock/shear zones and competent bedrock is interpreted as the fault or shear plane (Zhu et al., 2009; Arjwech et al., 2024). The rock mass within the shear zone is extensively fractured and contains higher water content than intact rock, which results in lower resistivity values (Meng et al., 2020; Sigdel and Adhikari, 2020; Tawir et al., 2025). Overall, the observed resistivity contrasts and shear zones indicate fault-related deformation, which can be correlated with the Badi Gad Fault, trending NE–SW with an estimated width of 20–40 m that traverses the landslide area.

5.3 X-ray diffraction analysis

The main clay mineralogical constituents of the soil along the landslide zone are determined by using XRD. The weathering degree assessment of rocks was of key interest due to the large

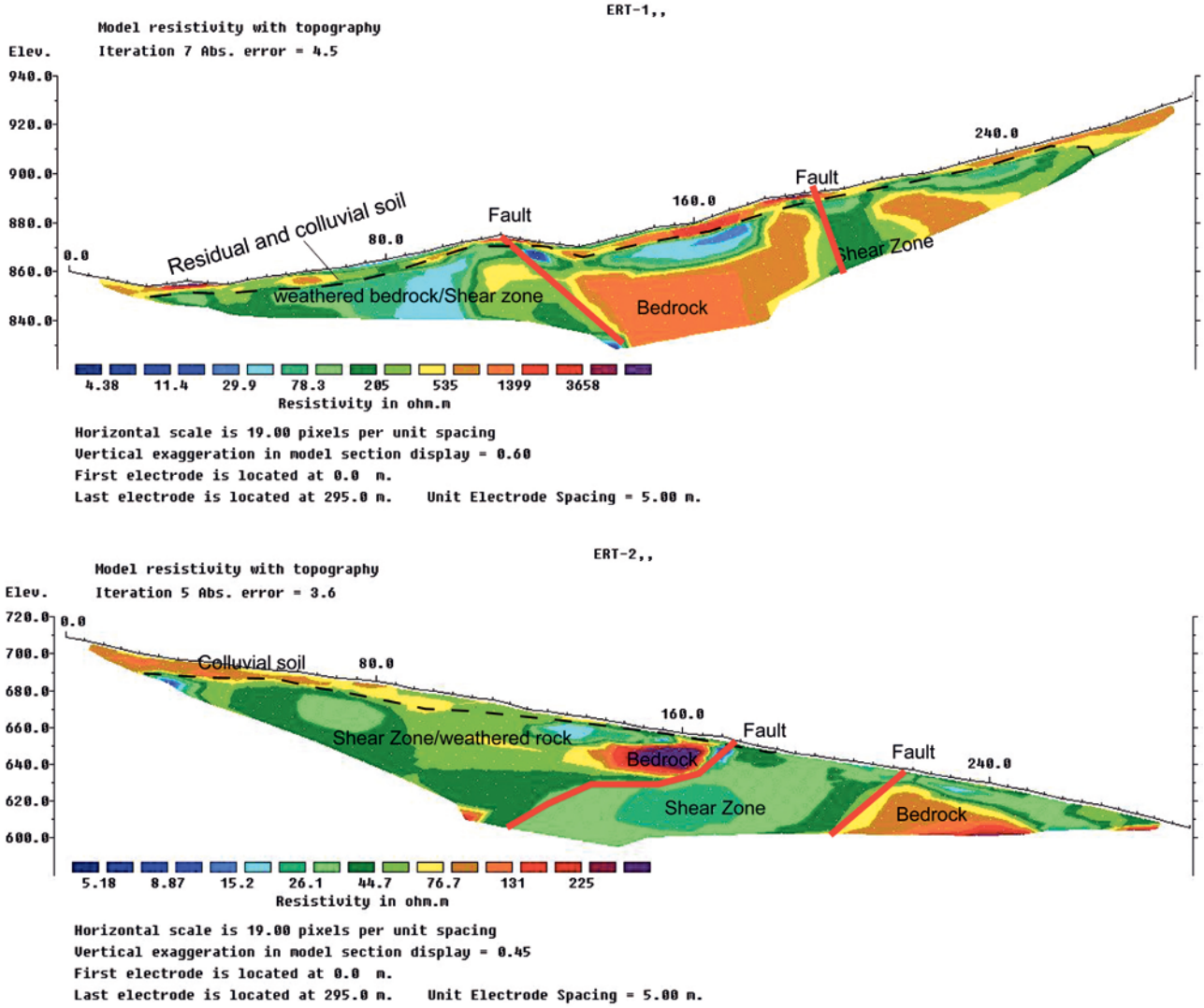

Fig.6 2D ERT tomogram of profile ERT 1 and ERT 2: The images show weathered shale and phyllite (low resistivity) separated by Intact bedrock of quartzite and phyllite (high resistivity) in both profiles. The red lines demarcate the presence of a sheared fault zone.

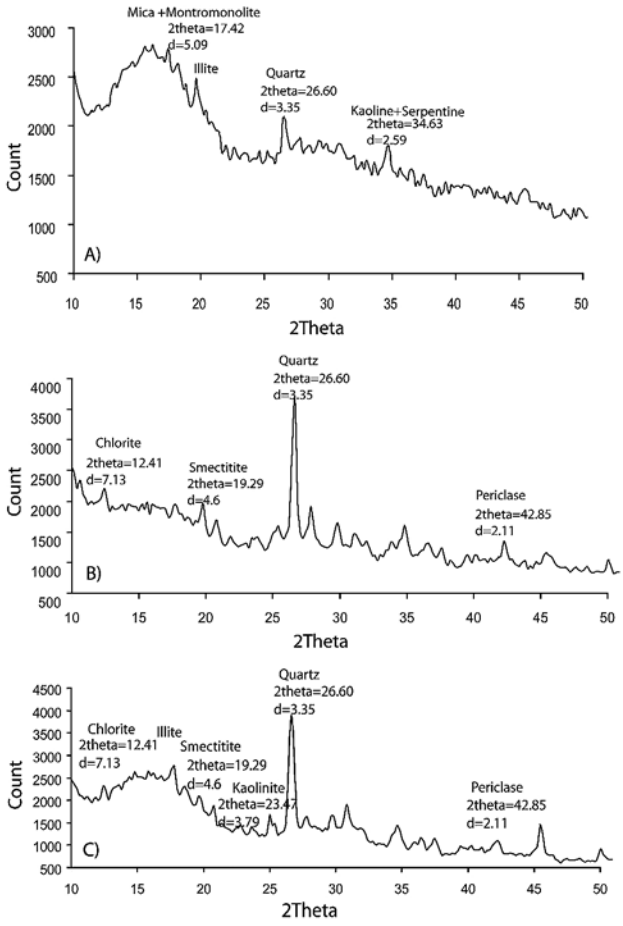

Fig.7: X ray diffraction (XRD) analysis of soil from the landslide area. The main clay minerals are illite, smectite and chlorite with dominant peak of Quartz.

aerial distribution and high weatherability of the rocks, which is visible in the field. The X-ray diffraction (XRD) pattern of the soil sample shows that the 2θ angle ranges from approximately 10° to 40°. The most prominent feature in this pattern is a distinct peak observed at 2θ = 26°, which is indicative of quartz, a common and stable mineral in weathered soils. The presence of quartz is consistent with the mineralogical composition typically derived from the mechanical weathering of metamorphic rocks such as phyllite and slate. In the lower 2θ angle region, particularly between 12° and 20°, the broad elevation in intensity without sharp, defined peaks suggests the presence of poorly crystalline clay minerals, such as kaolinite or illite. These clays often display diffuse peaks when they are present in small quantities or have undergone alteration, especially in natural landslide-affected soils. The lack of sharp basal reflections near 7.1° (typical of kaolinite) or 8.8° (typical of illite) that the clay content is relatively low and masked by the dominant quartz signal (Fig.7A). Similarly, a prominent and sharp peak at approximately 26.6° 2θ indicates a high content of quartz, which is commonly found in soils derived from metamorphic rocks such as slate and phyllite. In addition to quartz, several smaller peaks are observed in the lower angle range, particularly around 12.4° 2θ, which corresponds to a d-spacing of about 7.1 Å—this is characteristic of kaolinite or chlorite. The presence of peaks between 20° and 25° further supports the existence of kaolinite, while additional minor peaks around 35° to 38° suggest the possible presence of illite (Fig.7B).

The dominant clay minerals identified in the sample are quartz, chlorite, smectite, and kaolinite, with quartz showing the most intense peak at 2θ = 26.60°, indicating quartz as the most abundant mineral. Chlorite, shown at 2θ = 12.41° with moderate intensity, is a non-swelling clay but often forms in foliated or weathered metamorphic rocks. Its presence in moderate amounts implies a contribution to structural weaknesses, especially in schistose rocks, where it can reduce cohesion along foliation planes, aiding in the detachment of slope material during rainfall events. Smectite, identified at 2θ = 19.29°, shows a smaller but distinct peak, indicating it is present in lesser quantities than illite but still significant. Even in small amounts, smectite can greatly influence slope stability due to its high swelling and water retention capacity. Kaolinite, appearing at 2θ = 23.47°, shows a minor peak, indicating a lower abundance. It is non-expanding but can become plastic when wet, reducing shear strength and contributing to shallow slides (Fig.7C). Overall, the pattern suggests that quartz is the dominant crystalline phase, while kaolinite and possibly illite and smectite are present as secondary clay minerals. This mineralogical composition reflects a soil formed through moderate to advanced weathering, where resistant minerals like quartz remain, while feldspars and micas transform into clay minerals. Such a mineral assemblage is common in weathered slopes and landslide-prone terrains of the Lesser Himalayan region of Nepal (Regmi et al., 2012., Silwal et al., 2024).

5.4 Petrographical Analysis

The mineralogy, structural fabric, and textural features of rocks, including grain characteristics, fracture networks, and weathering by-products play a pivotal role in shaping rock behaviour and amplifying vulnerability to slope failure (Jaques et al., 2020). Based on petrographical analysis, we observe multiple interconnected features that indicate weathering of the minerals. The feldspar grains exhibit a cloudy texture and partial replacement by clay minerals.

Similarly, the flaky minerals outlined are most likely biotite, showing a V-shaped branching pattern that likely reflect structural deformation and cleavage propagation during alteration (Fig.8A). Such patterns often emerge as biotite begins to transform into chlorite or iron oxides, following cleavage planes. These flakes often darken at their margins or along fractures due to oxidation of iron within biotite showing progressive weathering (Torrent et al., 1980; Banfield & Murakami, 1998; Parsons et al., 2005) while biotite's transformation into fibrous chlorite and iron-rich coatings further affirms that the rock has undergone low-grade chemical alteration (Deer et al., 1992).

Similarly, elongated, sheet-like flaky minerals, likely biotite, exhibit distinct bending and kinking, which corresponds to folding and the development of foliation planes, most likely representing the S_1 fabric superimposed on an earlier, less deformed matrix (Fig.8B and 8D). The orientation and curvature of these micas suggest ductile deformation under differential stress (Shea and Kronenberg 1992; Rawling et al., 2002; Ping et al., 2011). In

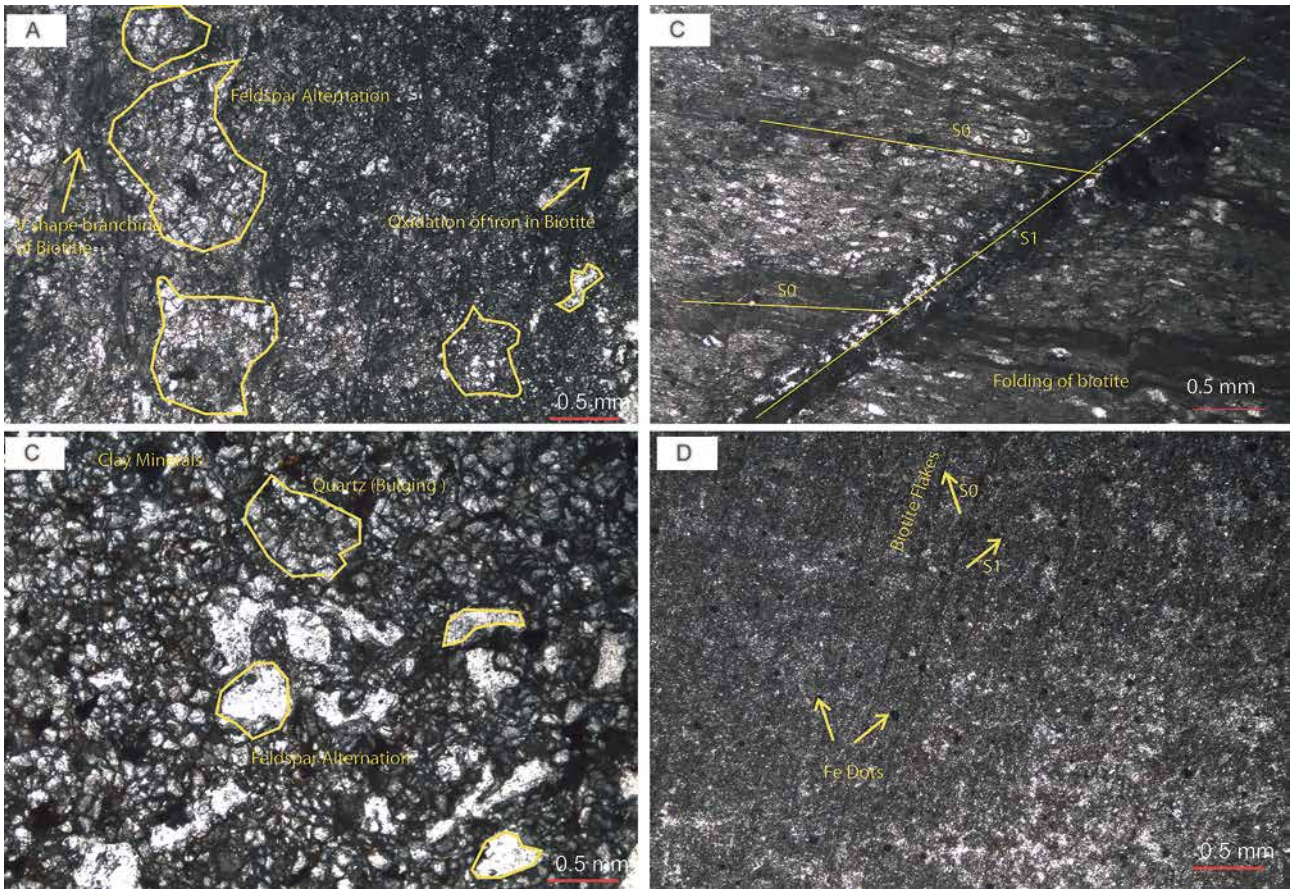

Fig.8: Photomicrographs of the different rock samples from landslide area A) Weathering of feldspar and branching pattern of biotite in Slate B) Alteration of felspar and Bulging quartz grains in slate C) Sheared biotite with S0 foliation plane cut by S1 structure in phyllite indicate the fault zone D) Sheet-like flaky minerals S_0 and S_1 structures with Fe bearing slate

several areas, possible shear planes or microfractures are visible, cutting across grains, these narrow linear features displace adjacent minerals slightly and are often accompanied by darkened edges, implying pathways for fluid infiltration and subsequent mineral alteration. Contrastingly, quartz grains appear clear and unaltered, maintaining sharp boundaries attesting to their resistance to chemical breakdown. (Fig.8C).

5.5 Geotechnical properties of soil

The geotechnical parameters include grain size distribution, Atterberg limits (liquid limit, plastic limit, plasticity index), moisture content and specific gravity. Besides these, strength parameters such as cohesion (c) and friction angle (ϕ) are crucial for evaluating the soil's shear strength and stability. Void ratio, porosity, and density further describe the soil's compactness and permeability characteristics. Lastly, unit weight is vital for understanding overburden stress and pressure distribution within soil layers (Table 1).

Grain Size Distribution

The grain size distribution of six soil samples (S1–S6) from the Birgha Bhanjyang landslide shows that the soils are mainly coarse-grained with 5–20% fines. Sample S4 has the highest fines, while S6 has the lowest. S1, S5, and S6 are well-graded with a broad particle size range, whereas S2, S3, and S4 are poorly graded sands (SP). Due to higher fines (15–20%), S2 and S4 are classified as silty sands (SP-SM) (Fig.9).

Moisture Content

The moisture content values for the soil samples show notable variability, reflecting differences in soil texture, permeability, and drainage characteristics across the landslide. The highest moisture content is observed in Sample S1 (14.53%), followed by S2 (12.58%), which are classified as well-graded sand (SW) and silty sand (SW-SM), respectively. These higher values suggest that these samples may retain more water, potentially due to finer material or higher porosity. Sample S5 (4.67%) and S6 (5.19%), despite having high sand and gravel content, show moderate moisture levels, likely influenced by limited fines and lower porosity. In contrast, the lowest moisture content is found in Samples S3 (0.73%) and S4 (0.67%), both classified as poorly graded sands (SP), which may be more compact or better drained (Table 1).

Specific Gravity

The specific gravity (Gs) of the samples ranges from 1.86 to 2.62, reflecting variable mineral composition and weathering. Low values in S5 (1.86), S1 (1.99), and S2 (1.95) indicate highly weathered soils with higher fines. Higher values in S6 (2.62)

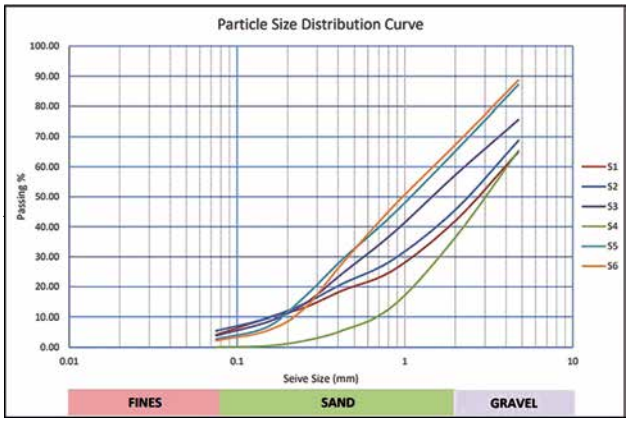

Fig. 9: Grain size distribution plot showing soil classification.

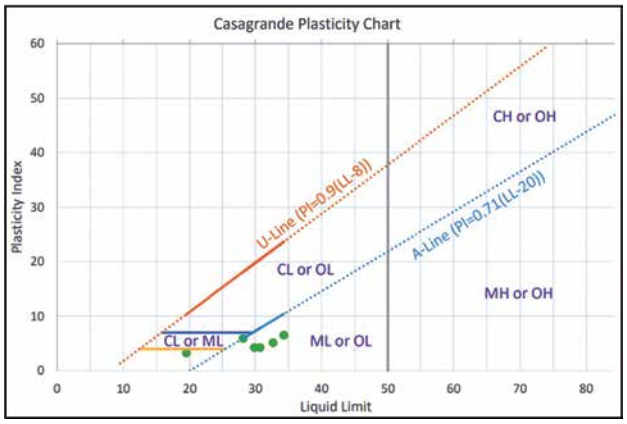

Fig. 10: The plasticity chart shows the classification of soils for this study

gesting clay with poor plasticity. This reflects limited cohesion in the fine fractions, typical of landslide materials (Table 1 and Fig.10).

Direct Shear Test

The results of the direct shear tests reveal that the soils are predominantly frictional with very low cohesive strength. Cohesion values are minimal, ranging from 0.041 kPa (S2) to 1.462 kPa (S4), indicating that the soils mainly consist of non-cohesive or weakly cohesive soils such as sands, gravels, and weathered colluvium. The internal friction angle (ϕ) varies considerably across the samples, from as low as 8.98° in S4 and S5 to a maximum of 18.83° in S1. Higher friction angles in S1, S2, and S3 suggest a denser, well-graded granular structure offering better shear resistance, while the lower friction angles in S4 and S5 point to looser, more weathered, or finer-grained materials with reduced strength (Table 1).

Table 1: Result of Engineering properties of soil samples collected from the landslide zone

Sample		S1	S2	S3	S4	S5	S6
Cu		25.69	23.34	13.33	9.32	7.22	6.44
Cc		2.01	1.41	0.82	0.63	0.64	1
% Gravel		35	31.25	24.31	12.17	11.3	34.62
% Sand		60.83	63.26	71.78	84.49	86.44	65.28
% Fines		4.17	5.49	3.91	2.72	2.26	0.1
Soil Type		SW	SW-SM	SP	SP	SP	SW
Moisture Content (%)		14.53	12.58	0.73	0.67	4.67	5.19
Specific Gravity		1.99	1.95	2.17	2.42	1.86	2.62
Strength Parameters	Cohesion (kPa)	0.052	0.041	0.062	1.198	1.467	0.785
	Friction Angle(ϕ°)	18.826	18.507	16.895	8.982	9.328	9.328
Liquid Limit		29.84	30.71	28.16	34.31	32.68	19.51
Plastic Limit		25.58	26.47	22.22	27.76	27.52	16.25
Plasticity Index		4.25	4.23	5.94	6.54	5.16	3.26
Void ratio		0.31	0.28	0.16	0.23	0.14	0.24
Porosity(n)		0.44	0.39	0.2	0.3	0.16	0.32
Density (gm/cm^3)		1.12	1.05	1.53	1.42	1.25	1.29
Unit Weight (KN/m^3)		11.2	10.29	14.99	13.91	12.25	12.64

6. DISCUSSION

This research examines the role of clay mineral composition, rock weathering, geological structures, and geotechnical characteristics in the formation of the Birgha Bhanjyang landslide. The dominant lithology in the area comprises highly weathered shale, and phyllite interbedded with thin beds of quartzite, which displays brittle deformation features. These rock masses are inherently prone to breakdown through mechanical weathering, and the slope is further weakened by the presence of the active Fault, i.e. Badi Gad Fault, a tectonic feature that has induced pervasive fracturing by long-term thrust activity. Evidence of faulting is revealed by the shear zone delineated in the ERT survey. The steep slope angles ranging from 50° to 80° aound the crown and body sections, where shear stress exceeds soil strength, while the gentler slopes at the toe (20°–30°) favor deposition of colluvium and accumulation of water, as seen in field evidence too. This configuration aligns with widely accepted observations that increasing slope angles directly correlate with greater landslide susceptibility (Lee and Min, 2001; Frattini et al., 2004).

Clay mineralogy plays a crucial role in the landslide dynamics in the area (Yalcin, 2007; Stead, 2015; Agung et al. 2017). Importantly, mineralogical analysis using X-ray Diffraction (XRD) reveals that weathering plays a crucial role not only in degrading rock mass strength but also in forming fine-grained materials such as clay mineral products that significantly influence slope stability. The XRD analysis shows that quartz is the dominant mineral, besides this, kaolinite or illite are also present in the landslide soil. The presence of illite over kaolinite suggests a greater likelihood of weak zones forming due to the chemical alteration of feldspar minerals (Baldermann et al., 2022). The weathering of feldspar, particularly within the interbedded shale and slate layers, exacerbates weathering during the monsoon season, making shale layers unstable and escalating the threat of landslides (Fredlund and Rahardjo, 1993). These clay minerals, especially kaolinite and illite, are commonly formed through the chemical weathering of phyllosilicate-rich rocks under moderate to intense weathering conditions (Islam et al., 2002; Islam et al., 2021). Illite and mica, although non-expansive, contribute to slope instability by promoting alignment of platy particles along potential

shear planes, which reduces internal friction and facilitates movement under stress (Parise et al., 2004). Chlorite and kaolinite, though lower in swelling potential, may still weaken slope material by increasing plasticity and lowering cohesion in wet conditions. These minerals tend to form microscopic to sub-microscopic crystals that can create clay-rich bands or horizons within weathered profiles (Chigira and Yokoyama, 2005). This weathering and clay formation is influenced by a fault that created a thick zone of weathered rock and clay minerals, making the area prone to debris flows during the monsoon season. Faults and thrusts significantly influence rock weathering, and this interplay is crucial in understanding landslide formation (Regmi et al., 2012; Bolla et al., 2020).

The weathering of the rocks is also supported by mineralogical analysis by thin section. The cloudy texture and partial replacement of feldspar grain by clay minerals, which appear as fine-grained, dusty material. This transformation signals chemical weathering under acidic, water-rich conditions (Wilson, 1984). Likely biotite shows a branching pattern which reflects structural deformation and cleavage propagation during alteration, such as biotite begins to transform into chlorite or iron oxides, following cleavage planes (Banfield & Murakami, 1998). These flakes often darken at their margins or along fractures due to oxidation of iron within biotite, a mark of progressive weathering (Gilkes and Suddhiprakar, 1979).

The geotechnical characteristics observed in the soil samples reflect significant weathering and mechanical alteration, likely associated with fault activity in a landslide-prone zone. The reduction in grain size distribution, especially the decreasing uniformity coefficient (Cu) from 25.69 in S1 to 6.44 in S6, and the low coefficients of curvature (Cc) below 1.5 in several samples (e.g., S3–S6), suggest intensive particle breakdown and sorting, which are typical of shear zone development in active fault zones (Caine et al., 1996; Xu et al., 2024). Such mechanical weathering results in poor gradation and weakened intergranular contacts, both of which contribute to reduced shear strength. The low value of cohesion (e.g., 0.052 kPa in S1 to just 0.041 kPa in S2, then slightly increasing in samples S4–S6) and the notably low friction angles (as low as 8.982° in S4) confirm that fault weathering has reduced the structural integrity of these soils (Sibson, 2003). These strength losses are commonly attributed to the formation of fine-grained materials (e.g., clay from feldspar weathering) by mechanical processes induced by fault movement. The Atterberg limits in samples S4 and S5 are also elevated (LL = 34.31% and 32.68%, respectively), suggesting the presence of clay minerals due to chemical weathering and mineral transformation near fault planes. The porosity and void ratio values also show notable trends, with higher porosities in S1 and S2 (0.44 and 0.39) that decrease towards S5 and S6, consistent with compaction and particle rearrangement in finer, weathered fault materials This is also supported by the variation in density and unit weight, where lower values (e.g., 1.05 g/cm^3 in S1) reflect the loose structure of fault-altered soils, whereas denser samples (e.g., 1.53 g/cm^3 in S3) suggest localized compaction or less weathered zones within the faulted terrain (Bray & Sancio, 2006). Furthermore, the weathered nature of the slope materials, confirmed by specific gravity values ranging from 1.86 to 2.62, indicates substantial mineralogical alteration and clay enrichment. The variation in specific gravity is consistent with the presence of weathered phyllites and clay-rich soils, whose lower density corresponds to increased porosity and water retention (Frattini et al., 2004).

These findings indicate that slope failure at Birgha Bhanjyang landslide is governed by weak lithology together with tectonic deformation caused by Badi Gad fault, which play a significant role in both mechanical and chemical weathering of rocks and soil.

7. CONCLUSION

Based on integrated geological, geophysical, mineralogical, and geotechnical investigations, the landslide is predominantly developed in weak residual soil composed of poorly graded sand with silt, pebbles, and cobbles. ERT profiling confirmed the presence of a low-resistivity shear zone and high-resistivity bedrock. The Badi Gad fault has played a key role in the deformation and weakening of the bedrock, enhancing the weathering process. Mineralogical analysis through XRD revealed a dominance of quartz with some other clay minerals, such as illite, chlorite and smectite formed during intense weathering, which reduce rock strength. The swelling behaviour of illite under wet conditions promotes progressive slope failure. The alteration of feldspar and biotite is clearly visible in petrographical analysis. Geotechnical tests further support the instability of the slope: soils are largely poorly graded sands (SP) with low cohesion and variable friction angles (8°–18°), and liquid limits ranging from 19% to 34%, indicating material inconsistency and these characteristics are matching of the soil of the active faulted area. At the endpoint, the combined influence of weak lithology, fault-controlled deformation, and mineral alteration makes the Birgha Bhanjyang landslide highly susceptible to failure.

Acknowledgement: The authors would like to thank Department of Mines and Geology (DMG) for providing petrographical analysis and geotechnical test of rock and soil samples. We would like to thank Nepal Academy of Science and Technology (NAST) for supporting XRD analysis.

References

Agung, P., Pramusandi, S., & Damianto, B., 2017: Identification and classification of clay shale characteristic and some considerations for slope stability. African Journal of Environmental Science and Technology, 11(4), 163–197.

Arjwech, R., Hongsresawat, S., Chaisuriya, S., Rattanawannee, J., Kanjanapayont, P., & Youngme, W., 2024: Identification and verification of the movement of the hidden active fault using electrical resistivity tomography and excavation. Geosciences, 14(8), 196. https://doi.org/10.3390/geosciences1408019

ASTM International, 2021: ASTM Volume 04.09 Soil and Rock (II): D5878–latest. Annual book of ASTM standards. ASTM International.

Baldermann, A., Banerjee, S., Czuppon, G., Dietzel, M., Farkaš, J., Löhr, S., Moser U., Scheiblhofer E., Wright N.M., Zack, T., 2022: Impact of green

clay authigenesis on element sequestration in marine settings. Nature Communications, 13, 1527.

Banfield, J. F., & Murakami, T., 1998: Atomic-resolution transmission electron microscope evidence for the mechanism by which chlorite weathers to 1:1 semi-regular chlorite-vermiculite. American Mineralogist, 83 (3–4), 348–357. https://doi.org/10.2138/am-1998-3-401

Bolla, A., Paronuzzi, P., Pinto, D., Lenaz, D., & Del Fabbro, M., 2020: Mineralogical and geotechnical characterization of the clay layers within the basal shear zone of the 1963 Vajont landslide. Geosciences, 10(9), 360. https://doi.org/10.3390/geosciences10090360

Bray, J. D., & Sancio, R. B., 2006 : Assessment of the liquefaction susceptibility of fine-grained soils. Journal of Geotechnical and Geoenvironmental Engineering, 132(9), 1165–1177. https://doi.org/10.1061/(ASCE)1090-0241(2006)132:9(1165)

Brenner, R., Garga, V., & Blight, G., 2012: Shear strength behaviour and the measurement of shear strength in residual soils. In G. Blight & E. Leong (Eds.), Mechanics of residual soils (2nd ed., pp. 155–190). CRC Press.

Calcaterra, D., & Parise, M., 2005: Landslide types and their relationships with weathering in a Calabrian basin, southern Italy. Bulletin of Engineering Geology and the Environment, 64, 193–207. https://doi.org/10.1007/s10064-005-0266-y

Calcaterra, D., & Parise, M. (Eds.), 2005: Weathering as a predisposing factor to slope movements. Geological Society, London, Engineering Geology Special Publications, 23, 1–4. https://doi.org/10.1144/EGSP23.1

Caine, J. S., Evans, J. P., & Forster, C. B., 1996: Fault zone architecture and permeability structure. Geology, 24(11), 1025–1028. https://doi.org/10.1130/0091-7613(1996)024

Chigira, M., & Sone, K., 1991: Chemical weathering mechanisms and their effects on engineering properties of soft sandstone and conglomerate cemented by zeolite in a mountainous area. Engineering Geology, 30(3–4), 195–219. https://doi.org/10.1016/0013-7952(91)90003-X

Chigira, M., & Yokoyama, O., 2005: Weathering profile of non-welded ignimbrite and the water infiltration behavior within it in relation to the generation of shallow landslides. Engineering Geology, 78(2–3), 187–207. https://doi.org/10.1016/j.enggeo.2005.01.008

Deer, W. A., Howie, R. A., & Zussman, J., 1992: An introduction to the rock-forming minerals (2nd ed.). Longman Scientific & Technical.

Dhital, M. R., 2015: Geology of the Nepal Himalaya: Regional perspective of the classic collided orogen. Springer. https://doi.org/10.1007/978-3-319-02496-7

Dhital, M. R., Paudel, S. R., & Arita, K., 2002: Geological study of the Lesser Himalaya in the Kusma-Baglung area, western Nepal. Journal of Nepal Geological Society, 28, 1–16.

Department of Mines and Geology (DMG), 1983: Geological map of western central Nepal 1:250,000. Department of Mines and Geology, Kathmandu, Nepal

Frattini, P., Crosta, G. B, Fusi, N., Negro P. D., 2004: Shallow landslides in pyroclastic soils: a distributed modelling approach for hazard assessment, Engineering Geology, 73, Issues 3–4, 277–295

Fredlund, D.G. and Rahardjo, H., 1993: Introduction of Soil Mechanics. Soil Mechanics for Unsaturated Soils. John Wiley and Sons, Inc., New York, 1–16. https://doi.org/10.1002/9780470172759

Hossain, S., Al Noor Tushar, M., Islam, S., et al., 2025: Investigating the role of rock weathering and clay mineralogy in landslide occurrences within the exposed Tertiary formations in Rangamati area. Geoenvironmental Disasters, 12, 20. https://doi.org/10.1186/s40677-025-00324-w

Indrawan, I. G. B., Tamado, D., Abrar, M., & Warmada, I. W., 2024: Mineralogical and Engineering Properties of Soils Derived from In Situ Weathering of Tuff in Central Java, Indonesia. Geosciences, 14(8), 213. https://doi.org/10.3390/geosciences14080213

Islam, M. R., Rojstaczer, S., Aario, R., & Peuraniemi, V., 2002 : Mineralogical changes during intense chemical weathering of sedimentary rocks in Bangladesh. Journal of Asian Earth Sciences, 20(8), 889–901. https://doi.org/10.1016/S1367-9120(01)00074-2

Islam, A., Khan, Z., Mazumder, A., Moslehuddin, A., Uddin, M., & Mori, Y., 2021: Clay mineralogy of soils from lower Atrai basin of Bangladesh. Dhaka University Journal of Biological Sciences, 30(2), 293–306. https://doi.org/10.3329/dujbs.v30i2.54654

Jaques, D. S., Marques, E. A. G., Marcello, L. C., Leão, M. F., Ferreira, E. P. S., & Lemos, C. C. S., 2020 : Changes in the physical, mineralogical, and geomechanical properties of a granitic rock from weathering zones in a tropical climate. Rock Mechanics and Rock Engineering, 53(9), 4131–4146. https://doi.org/10.1007/s00603-020-02240-x

Kumar, T., & Paudyal, K. R., 2018: Fault-controlled geomorphic features in Ridi-Shantipur area of Gulmi District and their implications for active tectonics. Journal of Nepal Geological Society, 55(Sp. Issue), 157–165.

Lee, S., & Min, K., 2001: Statistical analysis of landslide susceptibility at Yongin, Korea. Environmental Geology, 40(9), 1095–1113. https://doi.org/10.1007/s002540100310

Meng, F., Zhang, G., Qi, Y., Zhou, Y., Zhao, X., & Ge, K., 2020: Application of combined electrical resistivity tomography and seismic reflection method to explore hidden active faults in Pingwu, Sichuan, China. Open Geosciences, 12(1), 174–189. https://doi.org/10.1515/geo-2020-0040

Neupane, S., & Adhikari, R., 2011: Role of clay minerals in the occurrence of landslides along Narayangarh-Mugling Highway section, central Nepal. Journal of Nepal Geological Society, 43(Sp. Issue), 301–308. https://doi.org/10.3126/jngs.v43i0.25619

Paudel, L. P., 2012: Thin-skinned tectonics of the Tansen-Pokhara section, central Nepal Himalaya. Journal of Natural History Museum, 26, 15–28.

Panthee, S., Dulal, S., Pandey, V. H. R., Yadav, V., Singh, P. K., & Kainthola, A., 2023: Engineering geological characteristics and failure mechanics of Jure rock avalanche, Nepal. Geoenvironmental Disasters, 10(1), 1–16. https://doi.org/10.1186/s40677-023-00256-3

Parise, M. & Calcaterra, Domenico & Larsen, Matthew, 2004: Introduction to Weathering and Slope Movement papers. Quarterly Journal of Engineering Geology and Hydrogeology. 37. 76. 10.1144/1470-9236/04-200.

Parsons, R. L., Pullman, R. H., Ratcliff, I. W., Reinsch, T. G., Schoeneberger, P. J., & Yeck, R. D., 2005: Petrographic analysis of soils. In Soil survey laboratory methods manual (Soil Survey Investigations Report No. 42, Version 5.0, pp. 1–16). U.S. Department of Agriculture, Natural Resources Conservation Service.

Park, J., Jeong, S., Jang, S., Lee, J., Ko, K., & Yang, M., 2024: Influence of chemical weathering and microcracks on permeability variations in crystalline rocks. Water, 16(20), 3007. https://doi.org/10.3390/w16203007

Rawling, Geoffrey C., Patrick Baud, and Teng-fong Wong, 2002: Dilatancy, brittle strength, and anisotropy of foliated rocks: Experimental deformation and micromechanical modeling." Journal of Geophysical Research: Solid Earth 107, no. B10: ETG-8.

Regmi, A. D., Yoshida, K., Dhital, M. R. & Devkota. K., 2012: Effect of rock weathering, clay mineralogy, and geological structures in the formation of

large landslide: A case study from Dumre Besi landslide, Lesser Himalaya, Nepal. Landslides, 10(1), 1–13. https://doi.org/10.1007/s10346-011-0311-7

Sajinkumar, K.S., Anbazhagan, S., Pradeepkumar, A.P& Rani, V. R., 2011: Weathering and landslide occurrences in parts of Western Ghats, Kerala. Journal of Geological Society of India, 78, 249–257. https://doi.org/10.1007/s12594-011-0089-1

Sakai, H., 1985: Geology of the Kali Gandaki Supergroup of the Lesser Himalayas in Nepal. Memoirs of the Faculty of Science, Kyushu University, Series D: Geology, 25(3), 337–397.

Silwal, B. R., Gyawali, B. R., & Yoshida, K., 2024: Geochemical and mineralogical analysis of low-grade metamorphic rocks and their response to shallow landslide occurrence in Central Nepal. Geoenvironmental Disasters, 11(1), 1–16. https://doi.org/10.1186/s40677-024-00301-9=

Sigdel, A., & Adhikari, R. K., 2020: Application of Electrical Resistivity Tomography (ERT) survey for investigation of the landslide: a case study from Taprang landslide, Kaski district, west-central Nepal. Journal of Nepal Geological Society, 60, 103–115. https://doi.org/10.3126/jngs.v60i0.31261

Shea, William T., and Andreas K. Kronenberg, 1992: Rheology and deformation mechanisms of an isotropic mica schist." Journal of Geophysical Research: Solid Earth 97, no. B11: 15201-15237.

Stead, D., 2015: The influence of shales on slope instability. In D. Stead (Ed.), ISRM Congress (Paper No. ISRM-13CONGRESS). ISRM, Lisbon.

Sibson, R. H., 2003: Brittle-failure controls on maximum sustainable overpressure in different tectonic regimes. AAPG Bulletin, 87(6), 901–908. https://doi.org/10.1306/01290300181

Tawir, N., Lethy, A., Abbas, M., Abdel Fattah, T. H., Al-Maghraby, M., & Osman, M., 2025: Geological and geophysical evaluation of the subsurface conditions for establishing new dwelling area East New Cairo City. NRIAG Journal of Astronomy and Geophysics, 14(1), 36–50. https://doi.org/10.1080/20909977.2025.2449790

Torrent, J., Schwertmann, U., & Schulze, D. G., 1980: Iron oxide mineralogy of some soils of two river terrace sequences in Spain. Geoderma, 23(3), 191–208. https://doi.org/10.1016/0016-7061(80)90007-3

Vannucchi, P., Fisher, D. M., Bier, S., & Gardner, T. W., 2003: From seamount accretion to tectonic erosion: Formation of Osa Mélange and the effects of Cocos Ridge subduction in southern Costa Rica. Tectonics, 22(6), 1078. https://doi.org/10.1029/2002TC001474

Wang, L., Loew, S., Gu, X., & Lei, Q., 2024: Emergence of diverse failure patterns in weathering-induced landslides: Insights from high-fidelity particle finite element simulations. In EGU General Assembly 2024, Vienna, Austria, 14–19 Apr 2024 (EGU24-6969). Copernicus Meetings. https://doi.org/10.5194/egusphere-egu24-6969

Wilson, M. J., Bain, D. C., & Duthie, D. M. L., 1984 : The soil clays of Great Britain: II. Scotland. Clay Minerals, 19(5), 709–735. https://doi.org/10.1180/claymin.1984.019.5.03

Xu, Z., Ye, H., & Li, L., 2024: Particle size characteristics of sliding-zone soil and its role in landslide occurrence: A case study of the Lanniqing landslide in Southwest China. Frontiers in Earth Science, 12, 1483534. https://doi.org/10.3389/feart.2024.1483534

Yalcin, A., 2007: The effects of clay on landslides: A case study. Applied Clay Science, 38(1–2), 77–85. https://doi.org/10.1016/j.clay.2007.01.002

Yu, C., 2019: Modeling of fracture geometry alteration and fracture flow evolution under geostress and water-rock interaction. arXiv Preprint. arXiv:1904.05659

Zhang, X.-P., Wong, L. N. Y., Wang, S.-J., & Han, G.-Y. (2011):Engineering properties of quartz mica schist." Engineering geology 121, no. 3-4 : 135-149..

Zhu, T., Feng, R., Hao, J.-Q., Zhou, J.-G., Wang, H.-L., & Wang, S.-Q., 2009:The Application of Electrical Resistivity Tomography to Detecting a Buried Fault: A Case Study. Journal of Environmental and Engineering Geophysics14. 145-151. 10.2113/JEEG14.3.145.